# Depletion of the Bose-Einstein condensate in Bose-Fermi mixtures

# Depletion of the Bose-Einstein condensate in Bose-Fermi mixtures

Stephen Powell and Subir Sachdev
*Department of Physics, Yale University, P.O. Box 208120, New Haven, CT 06520-8120*

Hans Peter Büchler
*Institut für Theoretische Physik, Universität Innsbruck, Technikerstraße 25, A-6020 Innsbruck, Austria*



We describe the properties of a mixture of fermionic and bosonic atoms, as they are tuned across a Feshbach resonance associated with a fermionic molecular state. Provided the number of fermionic atoms exceeds the number of bosonic atoms, we argue that there is a critical detuning at which the Bose-Einstein condensate (BEC) is completely depleted. The phases on either side of this quantum phase transition can also be distinguished by the distinct Luttinger constraints on their Fermi surfaces. In both phases, the total volume enclosed by all Fermi surfaces is constrained by the total number of fermions. However, in the phase without the BEC, which has two Fermi surfaces, there is a *second* Luttinger constraint: the volume enclosed by one of the Fermi surfaces is constrained by the total number of *bosons*, so that the volumes enclosed by the two Fermi surfaces are separately conserved. The phase with the BEC may have one or two Fermi surfaces, but only their total volume is conserved. We obtain the phase diagram as a function of atomic parameters and temperature, and describe critical fluctuations in the vicinity of all transitions. We make quantitative predictions valid for the case of a narrow Feshbach resonance, but we expect the qualitative features we describe to be more generally applicable. As an aside, we point out intriguing connections between the BEC depletion transition and the transition to the fractionalized Fermi liquid in Kondo lattice models.

PACS numbers: 03.75.Hh, 71.35.Lk, 51.30.+i, 64.60.-i

## I. INTRODUCTION

The Feshbach resonance has emerged as a powerful tool in studying ultracold atoms in regimes of strong interactions. For two isolated atoms scattering off each other, the Feshbach resonance is a singularity in their scattering length due to the coupling of the atomic states to a molecular bound state.[1,2] The singularity (at $\nu = 0$) occurs as a function of the detuning $\nu$, which is a measure of the energy difference between the atomic and molecular states. The value of $\nu$ can be varied by an applied magnetic field, and this effectively allows one to tune the strength of the atomic interactions.

For systems in the thermodynamic limit, with a finite density of atoms, there is no singularity at $\nu = 0$. Nevertheless, the vicinity of $\nu = 0$ is a regime of interesting many body effects. For a Feshbach resonance between two identical fermionic atoms, the many body ground state changes from a Bose-Einstein condensate (BEC) of molecules ($\nu \ll 0$) to a Bardeen-Cooper-Schrieffer (BCS) superfluid descended from a Fermi gas of atoms ($\nu \gg 0$). It is important to note that there is no true fundamental distinction between the BEC and BCS states here, and so the two limits are connected by a smooth crossover. Recent experiments[3,4,5] on $^6$Li and $^{40}$K atoms have succeeded in observing the BEC of molecules.

The consequences of the two-body Feshbach resonance are very different for other atomic statistics. For a Feshbach resonance between two identical bosonic atoms, it has been argued recently[6,7] that there is indeed a sharp singularity, *i.e.* a quantum phase transition, in the many body system as a function of $\nu$. This singularity is not precisely at $\nu = 0$, but is shifted away from it; it is not directly a reflection of the singularity in the scattering length of two isolated atoms, but is a new many body effect. Here, the two limiting states are a BEC of molecules ($\nu \ll 0$) and a BEC of atoms ($\nu \gg 0$). Unlike the fermionic case above, these two states cannot be connected smoothly to each other. The fundamental distinction between these states becomes apparent upon examining the quantum numbers of the vortices in the condensate: the quantum of circulation differs by a factor of 2 in the two limits, being determined respectively by the mass of a molecule or of an atom.

In the present paper, we will consider the remaining case of a mixture of two distinct types of atoms, one fermionic and the other bosonic. Mixtures of fermionic $^6$Li and bosonic $^7$Li atoms were studied by Truscott *et al.*[8] and Schreck *et al.*,[9] and they succeeded in achieving simultaneous quantum degeneracy in both species of atoms. Recently, Feshbach resonances have been observed between bosonic $^{23}$Na and fermionic $^6$Li atoms by Stan *et al.*,[10] and between bosonic $^{87}$Rb and fermionic $^{40}$K atoms by Inouye *et al.*[11] So the time is clearly appropriate to examine the many body properties of such mixed Bose and Fermi gases across a Feshbach resonance, in which the fermionic molecule of the two unlike atoms can also reach quantum degeneracy.

Our primary result is that such a mixture of fermionic and bosonic atoms also has a quantum phase transition. Again this transition is a many body effect, and does not occur precisely at $\nu = 0$. We will map out the phase diagram as functions of $\nu$, temperature ($T$), and the densities of the atoms (see Figs. 1, 2, 3, 6) and also describe the strong consequences of thermal and quantum fluctuations in the vicinity of the phase transition. It is also

possible that the mixture phase separates: this will be studied in the Appendix, where we determine the region of instability to phase separation (see Fig. 9).

As in the Fermi-Fermi and Bose-Bose cases, the existence of a quantum phase transition for the Bose-Fermi case can be easily understood by characterizing the two limiting cases. For $\nu \gg 0$, there is a BEC of the bosonic atoms and a Fermi surface of the fermionic atoms. In contrast, for $\nu \ll 0$, there is a Fermi surface of the fermionic molecules. If the number of the fermionic ($N_f$) and bosonic ($N_b$) atoms are unequal to each other, for $\nu \ll 0$, there will also be some residual atoms which are not in molecules forming their own ground state: for $N_f > N_b$ the extra fermions will form a separate Fermi surface of atoms, while for $N_b > N_f$, the extra bosons will form an atomic BEC. We note that for $N_f > N_b$, scanning the detuning $\nu$ takes us between limits with and without an atomic BEC. Consequently there must be a critical detuning at which the atomic BEC is completely depleted, and all the bosonic atoms have been absorbed into molecules.

A novel feature of this quantum phase transition is that it can be entirely characterized in terms of the Luttinger constraints on the Fermi surfaces.

(*i*) Consider, first, the phase without the BEC with $\nu \ll 0$. Here, there are 2 Fermi surfaces, one with Fermi surface excitations which are primarily the fermionic atoms, while the other has Fermi surface excitations which are primarily the fermionic molecules. We establish in Section V that this phase obeys *two* Luttinger theorems: the atomic Fermi surface encloses a volume associated with precisely $N_f - N_b$ states, while the molecular Fermi surface encloses precisely $N_b$ states.

(*ii*) Now consider the phase with the BEC. When the BEC is small, this phase retains 2 Fermi surfaces, one primarily atomic and the other primarily molecular. However, now the volumes enclosed by these Fermi surfaces are not separately conserved; only the total volume enclosed by both Fermi surfaces is required to contain $N_f$ states. Eventually, for $\nu \gg 0$, the molecular Fermi surface disappears entirely, and only a single Fermi surface with $N_f$ states remains. The disappearance of the molecular Fermi surface (in the presence of a BEC) is a second quantum transition whose character we will also discuss briefly in Section VI.

This paper will determine the value of the critical $\nu$ for the BEC depletion transition, and describe critical fluctuations in its vicinity. At $T = 0$, we will find in Section VI that this critical point is generically in the universality class[12,13] of the density-driven superfluid-insulator transition with dynamic exponent $z = 2$. There is also an interesting quantum multi-critical point for $N_f = 2N_b$ at which the BEC depletion quantum transition has a different character: this we will also describe. At $T > 0$, the BEC depletion transition is in the universality class of the $\lambda$-transition of $^4$He, and so will display similar critical singularities: a peak in the specific heat, and anomalies in transport coefficients.

Our quantitative results are determined within a mean-field picture, whose applicability is restricted to the case of a 'narrow' Feshbach resonance, where the relevant coupling is sufficiently weak. We nonetheless expect our results to be at least qualitatively applicable to the (experimentally more common) 'wide' Feshbach resonance.

We also find an additional $T = 0$ quantum phase transition involving the disappearance of the molecular Fermi surface. As shown in Section VI, this is described by a $z = 2$ critical theory of free fermions.

While our work was in progress, we learnt of the work of Yabu *et al.*[14] who addressed some related issues, but only in the limit of infinitesimal coupling between the atomic and molecular degrees of freedom. We will note their limiting results in Section III.

We now outline the contents of the body of the paper.

First, in Section II, we define the model Hamiltonian that will be used throughout the rest of the paper. In Section III, we consider the limit of vanishing coupling, where a purely classical analysis can be used.[14]

Section IV finds the phase structure for finite coupling, treating quantum-mechanical effects using a mean-field approach. In Section V, we describe our results regarding Luttinger's theorem for the system. In Section VI, the mean-field result of Section IV is reproduced using a field-theoretical approach, which further allows us to characterize the critical properties of the transition.

In Sections VII and VIII, two corrections are calculated to the mean-field theory, which can be used to determine the validity of this approximation. In Section VII, the two-loop corrections to the free energy are found, while in Section VIII, higher orders in the coupling are included, within a low-density approximation.

In the Appendix, we consider the stability of the system against separation into two regions with differing densities. It is shown that the system is indeed stable for a broad range of parameters.

## II. BASIC DEFINITIONS

The system consists of bosonic atoms $b$ and fermionic atoms $f$ which combine to form fermionic molecules $\psi$. The energy, relative to the chemical potential $\mu$, is for the atoms

$$\xi^f = \epsilon^f - \mu^f = \frac{k^2}{2m^f} - \mu^f \tag{2.1}$$

$$\xi^b = \epsilon^b - \mu^b = \frac{k^2}{2m^b} - \mu^b \tag{2.2}$$

and for the molecule

$$\xi^\psi = \epsilon^\psi - \mu^\psi = \frac{k^2}{2m^\psi} - \mu^\psi + \nu \ , \tag{2.3}$$

including the detuning $\nu$. The masses obey $m^\psi = m^f + m^b$ and, because of the interaction, the chemical potentials are related by $\mu^\psi = \mu^f + \mu^b$.

The grand Hamiltonian is

$$\begin{aligned}\mathcal{H} &= \xi_k^f f^\dagger f + \xi_k^b b^\dagger b + \xi_k^\psi \psi^\dagger \psi \\ &\quad - g\,(\psi^\dagger f b + b^\dagger f^\dagger \psi) + \lambda\, b^\dagger b^\dagger b\, b\,, \end{aligned} \tag{2.4}$$

with implicit momentum integrals. We assume throughout that the fermion spin is polarized along some direction, so that both $f$ and $\psi$ are treated as spinless. The fourth term (in $g$) causes the bosonic and fermionic atoms to couple and form molecules, while the final term (in $\lambda$) is an interaction between pairs of bosons. We omit the interaction between fermions because the exclusion principle forbids $s$-wave scattering between identical fermions and we assume that the interaction between $f$ and $\psi$ will be less important than the coupling $g$.

Taking the dimensions of momentum and energy to be unity, $\dim[k] = \dim[E] = 1$, we have $\dim[\psi] = -\frac{3}{2}$ and the same for the operators $b$ and $f$. (Throughout, we shall measure temperature, energy and frequency in the same units, so that $\hbar = k_{\rm B} = 1$.) The coupling constants have dimensions $\dim[g] = -\frac{1}{2}$ and $\dim[\lambda] = -2$.[27]

At temperature $T = 1/\beta \neq 0$, we have six dimensionless parameters. First let $N_b$ be the total density of bosonic atoms, including those bound in molecules, and let $N_f$ be the same for fermionic atoms. (We consider a unit volume, so that density is synonymous with number.) In the absence of any fermions, the bosons would condense at a temperature

$$T_0 = \frac{2\pi}{m^b}\left[\frac{N_b}{\zeta(\frac{3}{2})}\right]^{\frac{2}{3}}\,. \tag{2.5}$$

We can take as dimensionless parameters $T/T_0 = \beta_0/\beta$, $N_f/N_b$, $m^f/m^b$, $\nu/T_0$, $\gamma^2/T_0$ and $\lambda^2(m^b)^3 T_0$, where

$$\gamma = \frac{g^2}{8\pi}\left(\frac{2m^f m^b}{m^\psi}\right)^{3/2}\,. \tag{2.6}$$

In what follows, it will not usually be necessary to take account of the coupling between bosons given by the final term of (2.4). Except within the condensed phase, which will be treated in Section IV, the only effect of $\lambda$ is a renormalization of the boson mass, which we assume has already been incorporated into the definition of $m^b$.

### A. Physical units

In order to relate these parameters to experimental values, we may choose a unit of volume of $10^{-15}\,{\rm cm}^3$, which gives the unit of momentum as roughly $10^{-27}\,{\rm kg\cdot m/s}$. Taking the unit of mass to be 6 amu, corresponding to a lithium-6 atom, the unit of energy is roughly $7\times10^{-10}\,{\rm eV}$ or $8\,\mu{\rm K}$.

For a Feshbach resonance, we assume the expression[15]

$$g = \sqrt{\frac{2\pi a_{\rm bg}\,\Delta B \Delta\mu}{m}}\,, \tag{2.7}$$

where $a_{\rm bg}$ is the background scattering length, $\Delta B$ is the width of the resonance and $\Delta\mu$ is the difference in magnetic moments. For the values of $\Delta B = 1\,{\rm G}$, $\Delta\mu = \mu_{\rm B}$, the Bohr magneton, we find $a_{\rm bg} = 36 a_0$ (with $a_0$ the Bohr radius), for the case $g = 1$. This is not an unreasonable value, although somewhat lower than typical experimental values.[16] For a boson density $N_b = 10^{15}\,{\rm cm}^{-3}$ and mass $m_b = m_f = 6\,{\rm amu}$, the value $g = 1$ gives a dimensionless coupling of $\gamma^2/T_0 = 5\times10^{-4}$.

A calculation of the molecular propagator in the vacuum (see Section VIII, for instance) shows that the constant $\gamma$ is in fact the parameter that determines the width of the Feshbach resonance. Since the relevant energies are on the order of $T_0$, the condition for a narrow resonance is that $\gamma^2/T_0 \ll 1$. For the numerical results throughout this paper, we will always remain in this limit.

Following Ref. 7, we take

$$\lambda = \frac{2\pi}{m^b} a_{bb}\,, \tag{2.8}$$

where $a_{bb}$ is the scattering length for the boson-boson interaction. From Ref. 9, we take $a_{bb} = 5a_0$, which gives

$$\lambda^2 (m^b)^3 T_0 = 2\times10^{-3}\,. \tag{2.9}$$

The detuning $\nu$ appearing in the molecular dispersion relation (2.3) is given by[15]

$$\nu = \Delta\mu (B - B_0)\,, \tag{2.10}$$

where $B_0$ is the magnetic field at resonance and $B$ is the applied field.

## III. THE LIMIT $g \to 0$

The case of vanishing coupling, which can be addressed with a classical approach, has been considered by Yabu *et al.*[14] (The results presented in this section produce Fig. 3 of Ref. 14, which corresponds to our Fig. 3, below.)

For simplicity, we restrict the analysis to zero temperature, but similar arguments can be made for nonzero temperatures. We call the two Fermi energies $\epsilon_0^f$ and $\epsilon_0^\psi$, and the corresponding wavenumbers $k_0^f$ and $k_0^\psi$. At zero temperature, all bosons are at $\epsilon^b = 0$ and fermionic atoms or molecules must be added at their respective Fermi levels.

The atomic Fermi surface (FS) vanishes when all the fermionic atoms are contained in molecules, so that

$$k_0^\psi = (6\pi^2\, N_f)^{1/3}\,. \tag{3.1}$$

(The number of states within a unit sphere in momentum space is $1/6\pi^2$.) For this arrangement to be favorable energetically, the molecular Fermi energy, $\epsilon_0^\psi$, must remain

below the lowest atomic energy level. The boundary of the phase without an atomic FS is therefore where

$$\frac{1}{2m^\psi}(N_f)^{2/3} + \frac{\nu}{(6\pi^2)^{2/3}} = 0 \; . \tag{3.2}$$

Similarly, the molecular FS vanishes at the point when

$$\frac{1}{2m^f}(N_f)^{2/3} - \frac{\nu}{(6\pi^2)^{2/3}} = 0 \; . \tag{3.3}$$

The atomic (molecular) FS is therefore only absent for negative (positive) detuning $\nu$.

To find the boundary of the phase with a BEC, we must consider the depletion of the condensate. Bosons will take fermions and form molecules as long as their final energy is lower, *i.e.* $\epsilon_0^\psi < \epsilon_0^f + 0$. The phase boundary is therefore where $\epsilon_0^f = \epsilon_0^\psi$, which gives

$$\frac{1}{2m^f}(N_f - N_b)^{2/3} - \frac{1}{2m^\psi}(N_b)^{2/3} = \frac{\nu}{(6\pi^2)^{2/3}} \; , \tag{3.4}$$

where the wavenumbers have been determined from $N_b$ and $N_f$, using the fact that there is no condensate.

It should be noted that, in this limit, the coupling to fermionic atoms reduces the tendency of the bosons to condense. (The same is true at nonzero temperature.)

## IV. MEAN-FIELD THEORY

It is possible to go beyond the classical analysis used for vanishing coupling, by using mean-field theory. We will present here two parallel developments, in this section and Section VI, respectively. The first is based on single-particle quantum mechanics, using the mixing between the fermionic dispersion relations caused by the presence of a BEC. The second uses a field-theoretic approach and considers perturbative corrections to the bosonic propagator. The former has the advantage of giving a somewhat clearer physical picture and leading more directly to thermodynamic results (such as the question of phase separation, considered in the Appendix), while the latter leads naturally to higher-order corrections.

In the remainder of this section, we present the quantum-mechanical approach, starting from the Hamiltonian (2.4). First, in Section IV A, we make a mean-field approximation and diagonalize the new Hamiltonian. We then find the condition that a BEC should be energetically favorable, within this approximation.

Since the Hamiltonian is defined in the grand canonical ensemble, we must then relate the chemical potentials to the particle numbers, in Section IV B. Within the mean-field approximation, it is sufficient to find this relation to order zero in the coupling, neglecting two-loop corrections to the free energy.[17] Later, in Section VII, we determine the higher-order corrections.

In Section IV C, we restrict our attention to the case of zero temperature, where transitions occur between states with different numbers of Fermi surfaces. We identify the positions of these transitions and present the full phase diagram for $T = 0$.

### A. Mean-field Hamiltonian

Replacing the boson field $b$ in (2.4) by a real constant $\varphi$ gives

$$\begin{aligned} \mathcal{H}_{\rm mf} \;&=\; \xi_k^f f^\dagger f + \xi_k^\psi \psi^\dagger \psi - g\varphi(\psi^\dagger f + f^\dagger \psi) \\ &\quad - \mu^b \varphi^2 + \lambda \varphi^4 \; , \end{aligned} \tag{4.1}$$

which can be diagonalized to

$$\mathcal{H}_{\rm mf} = \xi_k^F F^\dagger F + \xi_k^\Psi \Psi^\dagger \Psi - \mu^b \varphi^2 + \lambda \varphi^4 \; . \tag{4.2}$$

The dispersion relations for the mixed fermions $F$, $\Psi$ are

$$\xi_k^{F,\Psi} = \tfrac{1}{2}\left(\xi_k^f + \xi_k^\psi\right) \pm \tfrac{1}{2}\sqrt{\left(\xi_k^f - \xi_k^\psi\right)^2 + 4g^2\varphi^2} \; , \tag{4.3}$$

with the choice that $\xi_k^F \geq \xi_k^\Psi$ for all $k$.

Since the mixing will cause the dispersion relations to separate, the total energy of the fermions is lowered by nonzero $\varphi$. This quantum-mechanical effect, in contrast to the purely classical effect described in Section III, therefore acts to favor condensation.

We must analyze the energetics to determine the point at which a condensate becomes favorable. The grand free energy $\Phi$ is minimized at temperature $1/\beta$ by a Fermi-Dirac distribution of each fermionic species $x$ ($x \in \{F, \Psi\}$). Ignoring the thermal distribution of bosons, which does not depend on $\varphi$, the total free energy is

$$\Phi(\varphi) \;=\; -\mu^b \, \varphi^2 \;+\; \lambda \, \varphi^4 \;+\; \sum_{x \in \{F,\Psi\}} R^x(\varphi) \; , \tag{4.4}$$

where

$$R^x(\varphi) = -\frac{1}{\beta} \int \frac{d^d k}{(2\pi)^d} \, \ln\left(1 + e^{-\beta \xi_k^x}\right) \; . \tag{4.5}$$

The phase transition to a state with nonzero $\varphi$ occurs when the quadratic coefficient changes sign, *i.e.* when

$$\Delta \equiv \frac{1}{2} \frac{d^2\Phi}{d\varphi^2}\bigg|_{\varphi=0} = 0 \; . \tag{4.6}$$

Specifically, for negative $\Delta$, nonzero $\varphi$ is energetically favored, so that the condensed phase is stable. Using (4.3), (4.4) and (4.5), we find

$$\Delta = -\mu^b + g^2 \int \frac{d^d k}{(2\pi)^d} \, \frac{n_{\rm F}(\xi_k^f) - n_{\rm F}(\xi_k^\psi)}{\xi_k^f - \xi_k^\psi} \; , \tag{4.7}$$

where $n_{\rm F}$ is the Fermi-Dirac distribution function. The integral equation $\Delta = 0$ may be solved numerically.

### B. Particle numbers

Since experiments are necessarily performed at fixed particle number, the expressions for the numbers in terms of the chemical potentials must be found. Particles of the species $b$, $f$ and $\psi$ are not independently conserved, so the relevant quantities are $N_f$ and $N_b$, the total numbers of fermionic and bosonic atoms, respectively (including those contained in molecules).

As mentioned above, it is sufficient within mean-field theory to determine these numbers to order zero in the coupling. Since the species $F$ and $\Psi$ each contain one atomic fermion, we have

$$N_f = \int \frac{d^d k}{(2\pi)^d} \left[ n_{\rm F}(\xi_k^\Psi) + n_{\rm F}(\xi_k^F) \right] . \qquad (4.8)$$

The number of bosons is (with $n_{\rm B}$ the Bose-Einstein distribution function)

$$N_b = \varphi^2 + \int \frac{d^d k}{(2\pi)^d} \left[ n_{\rm B}(\xi_k^b) \; + \; n_{\rm F}(\xi_k^\Psi) \cos^2\theta_k \right. \qquad (4.9)$$
$$\left. + \; n_{\rm F}(\xi_k^F) \sin^2\theta_k \right] ,$$

where the first term represents the condensate, the first term in the integrand is the thermal distribution of the bosons, and $\theta_k$ is the mixing angle.[28]

When $\varphi = 0$, such as along the boundary to the phase without a BEC, the expression for the number of bosons simplifies to

$$N_b = \int \frac{d^d k}{(2\pi)^d} \left[ n_{\rm B}(\xi_k^b) + n_{\rm F}(\xi_k^\psi) \right] . \qquad (4.10)$$

To locate this phase boundary for fixed particle numbers, we must find the values of $\mu^f$ and $\mu^b$ which give the required numbers and also satisfy $\Delta = 0$. (Of course, a third parameter must be tuned to its critical value to satisfy these three conditions simultaneously.)

Results from such a procedure are displayed in Fig. 1, which shows the boundary for $N_f/N_b = 1.11$ as a function of the detuning $\nu$ and temperature $T = 1/\beta$. The masses of the atoms are equal, $m^f = m^b$, and the solid line has dimensionless coupling $\gamma^2/T_0 = 2.5 \times 10^{-4}$. For comparison, the case of vanishing coupling, treated in Section III, is also shown with a dashed line. Both curves reach the value $T = T_0$, as in the case of free bosons, for $\nu \to \infty$, when molecules cannot be formed.

In Fig. 2 the same phase boundary is shown on a graph of fermion number versus detuning, for three different temperature values. The solid line is at zero temperature, $T = 0$, while the two dashed lines have nonzero temperatures. The coupling is $\gamma^2/T_0 = 2.5 \times 10^{-4}$ and the masses are equal, $m^f = m^b$. As expected, Bose condensation is favored by lower temperatures, as in the case of an isolated Bose gas.

It remains to be shown that the system is stable against separation into regions with different densities. It is shown in the Appendix that it is indeed stable for a large range of parameter values.

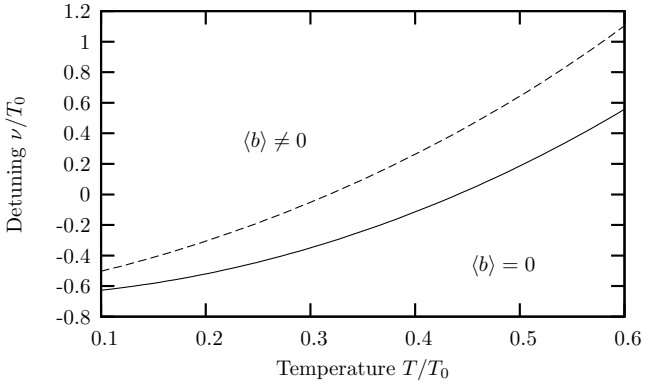


FIG. 1: Phase boundary with detuning $\nu$ and temperature $T$, for fixed particle numbers $N_f/N_b = 1.11$. The dashed line has vanishing coupling and has been found with a purely classical analysis. The solid line has dimensionless coupling $\gamma^2/T_0 = 2.5 \times 10^{-4}$, and has been determined using the mean-field theory of Section IV. For both, the condensed phase is on the left-hand side (for lower $T$) and labeled by $\langle b \rangle \neq 0$.

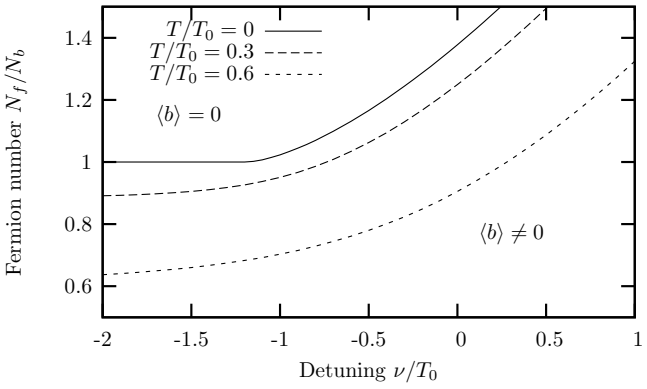


FIG. 2: Phase boundary with fermion number $N_f$ and detuning $\nu$, for three different temperatures. The coupling is $\gamma^2/T_0 = 2.5 \times 10^{-4}$ and the masses are equal, $m^f = m^b$. The two phases are labeled as in Fig. 1, with the condensed phase favored for higher detuning, lower fermion number and lower temperature.

### C. Zero-temperature phases

At $T = 0$, the Fermi-Dirac distribution function is replaced by a unit step and all bosons occupy the lowest-energy state. As noted by Yabu *et al.*,[14] the phase diagram can be further divided into a region with two Fermi surfaces and a region with a single Fermi surface. (We ignore the trivial case without any Fermi surfaces, which requires $N_f = 0$.)

Except when the atomic numbers precisely match, $N_f = N_b$, the case of a single surface can only occur when there is a BEC. In this case, $\varphi$, the expectation value of $b$, is given by the minimum of the free energy $\Phi$

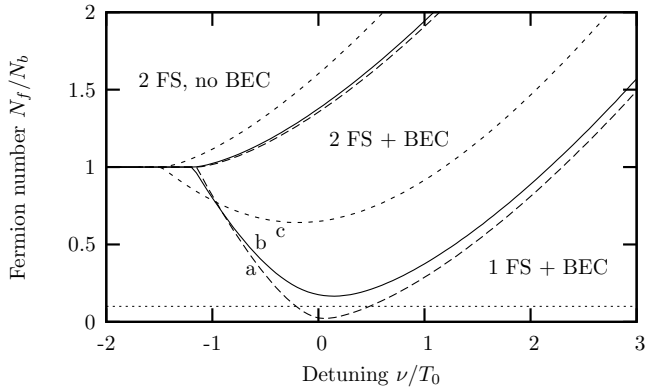


FIG. 3: The phase diagram at $T = 0$ with dimensionless couplings (a) $\gamma^2/T_0 = 10^{-6}$, (b) $\gamma^2/T_0 = 2.5 \times 10^{-4}$ and (c) $\gamma^2/T_0 = 2.0 \times 10^{-2}$. The atomic masses have been taken to be equal, $m^f = m^b$ and the coupling between bosons is given by $\lambda^2(m^b)^3 T_0 = 2 \times 10^{-3}$. The three distinct phases have, respectively, no Bose-Einstein condensate and two Fermi surfaces (labeled '2 FS, no BEC'), a condensate and two Fermi surfaces ('2 FS + BEC'), and a condensate and a single Fermi surface ('1 FS + BEC'). The dotted line indicates the fermion number at which Fig. 4 is plotted.

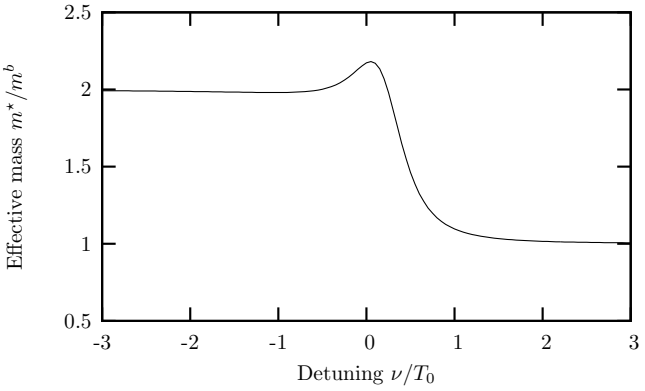


FIG. 4: The effective mass $m^\star$ at the Fermi surface, with fermion number $N_f = 0.1N_b$, coupling $\gamma^2/T_0 = 2.5 \times 10^{-4}$ and equal atomic masses $m^f = m^b$. As can be seen from the dotted line in Fig. 3, these parameters give a phase with a single Fermi surface. This surface changes from having a molecular character, with $m^\star \simeq m^\psi$, to having an atomic character, $m^\star \simeq m^f$.

given in (4.4), so that we must solve

$$-2\mu^b \varphi \;+\; 4\lambda \varphi^3 \;+\; \sum_{x\in\{F,\Psi\}} \frac{dR^x}{d\varphi} \;=\; 0 \qquad (4.11)$$

(excluding the root $\varphi = 0$).

Following the choice that $\xi_k^F \geq \xi_k^\Psi$ in (4.3), the second Fermi surface disappears when $\xi_{k=0}^F = 0$, making the Fermi wavenumber for $F$ fermions vanish. For this to be the case, we require $\mu^f > 0$, $\mu^\psi > \nu$ and

$$g\varphi = \sqrt{\mu^f(\mu^\psi - \nu)}\,, \qquad (4.12)$$

which should be solved simultaneously with (4.11).

These expressions, along with the results in Section IV B for the particle numbers, allow the complete zero-temperature phase diagram to be plotted. In Fig. 3, the phase boundaries are shown on a graph of fermion number against detuning, for equal atomic masses $m^f = m^b$. The three sets of boundaries have couplings (a) $\gamma^2/T_0 = 10^{-6}$, (b) $\gamma^2/T_0 = 2.5\times10^{-4}$ and (c) $\gamma^2/T_0 = 2.0\times10^{-2}$. (Since the dimensionless coupling depends on the fourth power of the coupling $g$ appearing in the Hamiltonian, these large changes in $\gamma^2/T_0$ in fact correspond to changes in $g$ of only factors of 4 and 3 respectively. All of these coupling values are within the narrow resonance regime.) Throughout, we take $\lambda^2(m^b)^3T_0 = 2 \times 10^{-3}$.

The boundaries divide the diagram into three regions, depending on the presence of a condensate and the number of Fermi surfaces. In the region labeled '2 FS, no BEC', the discriminant $\Delta$ is positive, so there is no BEC and two Fermi surfaces. In the region labeled '2 FS + BEC', $\Delta$ is negative and there is a condensate, as well as two Fermi surfaces. The lowermost region of the diagram, labeled '1 FS + BEC', has a condensate and only a single Fermi surface.

In the limit of vanishing coupling (as in Ref. 14 and Section III), the boundary between the regions with one and two Fermi surfaces extends down to the line $N_f = 0$. The region with a single Fermi surface is then divided into two, with the left-hand side having a Fermi surface of molecules and the right-hand side a Fermi surface of atoms. Including the quantum-mechanical effects, these two regions are no longer distinct, with the single Fermi surface crossing over from having a molecular character on one side (lower $\nu$) to having an atomic character on the other (higher $\nu$).

This crossover is illustrated in Fig. 4, where the effective mass $m^\star$ at the Fermi surface is plotted. The fermion number is set at $N_f = 0.1N_b$ and the coupling is $\gamma^2/T_0 = 2.5 \times 10^{-4}$, so that the system is within the phase with a single Fermi surface (of $\Psi$ fermions). The effective mass is defined as

$$m^\star = \left( \frac{d^2\xi_k^\Psi}{dk^2}\bigg|_{k_0^\Psi} \right)^{-1} . \qquad (4.13)$$

For $\nu \ll 0$, the Fermi surface has an essentially molecular character and $m^\star \simeq m^\psi$, while for $\nu \gg 0$, it is atom-like, with $m^\star \simeq m^f$.

In Fig. 5, the Fermi wavenumbers of the two fermionic species are plotted, for coupling $\gamma^2/T_0 = 2.5 \times 10^{-4}$ and two different fermion numbers, $N_f = \frac{3}{2}N_b$ (solid lines) and $N_f = \frac{1}{2}N_b$ (dashed lines). In both the phase without a condensate (solid lines for $\nu/T_0 < 0.25$) and the phase with a single Fermi surface (solid lines for $\nu/T_0 > 2.9$, dashed lines for $\nu/T_0 < -0.65$ and $\nu/T_0 > 1.3$) the wavenumbers are constant, due to the fixed particle numbers. Only in the phase with two Fermi surfaces and a

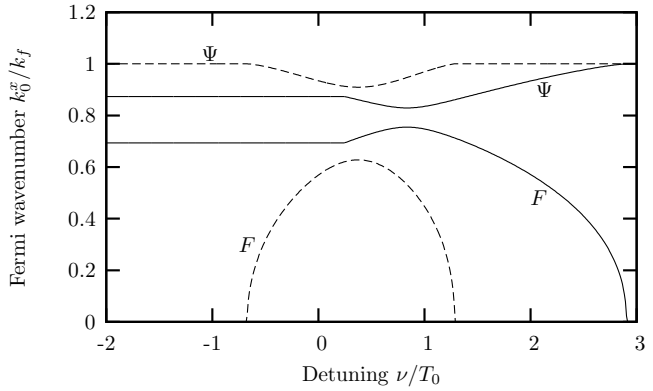


FIG. 5: The Fermi wavenumbers for the two mixed species of fermions, $\Psi$ and $F$, with coupling $\gamma^2/T_0 = 2.5 \times 10^{-4}$ and equal atomic masses $m^f = m^b$. The solid lines have fermion number $N_f = \frac{3}{2}N_b$, while the dashed lines have $N_f = \frac{1}{2}N_b$. As can be seen in Fig. 3, the solid line goes between all three phases (at $\nu/T_0 \simeq 0.25$ and $\nu/T_0 \simeq 2.9$), while the dashed line goes from the phase with a single Fermi surface to that having two and back again (at $\nu/T_0 \simeq -0.65$ and $\nu/T_0 \simeq 1.3$). The wavenumbers are measured in units of $k_f$, the Fermi wavenumber for free fermions with number $N_f$.

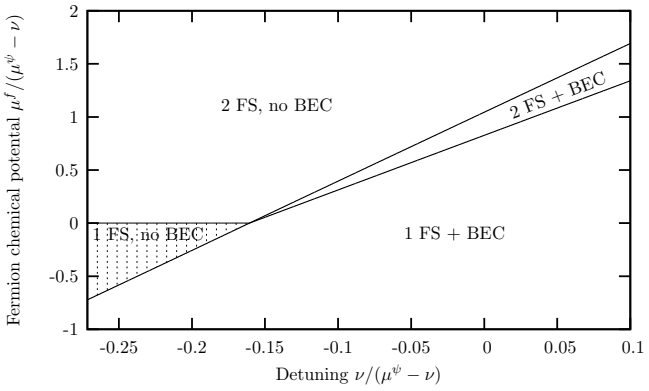


FIG. 6: The phase diagram with the fermion chemical potential $\mu^f$ plotted on the vertical axis and the detuning $\nu$ on the horizontal axis. Both have been scaled to $\mu^\psi - \nu$, which is held fixed throughout the plot. The boundary between 2 FS, no BEC and 1 FS + BEC in Fig. 3 expands into a new phase, labeled '1 FS, no BEC', within which there are only molecules, whose density is constant (both $N_f$ and $N_b$ remain fixed in the shaded region). The atomic masses are equal, $m^f = m^b$, and the couplings are $\gamma^2/T_0 = 2.5 \times 10^{-4}$ and $\lambda^2(m^b)^3 T_0 = 2 \times 10^{-3}$. (Since the boson density is not fixed in this plot, the value of $T_0$ appropriate to the phase 1 FS, no BEC has been used to define the dimensionless couplings.)

BEC do the Fermi wavevectors change with detuning. (At the fermion number used in Fig. 4, the system stays in the phase with a single Fermi surface throughout and $k_0^\Psi = k_f$, $k_0^F = 0$ for all detunings.)

We now turn our attention to the line dividing the phases 2 FS, no BEC and 1 FS + BEC in Fig. 3. This boundary is horizontal and starts at the point where the three phases meet; in Section V A, we will prove that this is at exactly $N_b = N_f$. At this transition, two changes occur: both the second Fermi surface vanishes and the BEC appears, as the line is crossed from above. Physically, this results from the fact that molecules are highly energetically favored in this region, so that as many molecules as possible are formed, and the residual atoms form their ground state. For $N_f > N_b$, these atoms are fermionic and form a Fermi surface, while for $N_f < N_b$, they are bosonic and form a condensate. Precisely at $N_f = N_b$, there are no residual atoms, so that there is no condensate and only a molecular Fermi surface.

This situation is illustrated by Fig. 6, which shows the same phase diagram as Fig. 3, but with the chemical potential for the fermionic atoms, $\mu^f$, on the vertical axis. Throughout the plot $\mu^\psi - \nu$, and hence the Fermi wavenumber for the molecules, $k_0^\psi$, is held fixed. In the region where $\mu^f > 0$, the essential features are unchanged, with the same three phases as shown in Fig. 3. The boundary between the phases 2 FS, no BEC and 1 FS + BEC, however, is seen to extend into an entire phase, labeled '1 FS, no BEC'. In this region, there is no condensate and $\mu^f$ is negative, so that there is only one Fermi surface, of molecules. This entire phase therefore has $N_f = N_b$ and collapses onto a single line in Fig. 3. Moreover, because $k_0^\psi$ is constant, $N_f$ and $N_b$ are both fixed in this phase. The situation in the shaded region of Fig. 6 resembles that in the Mott insulator lobes in the phase diagram of the boson Hubbard model (see Ref. 12 and Chapter 10 of Ref. 13); at fixed $\mu^\psi$, the density of particles is insensitive to the variation in the chemical potential $\mu^f$.

## V. LUTTINGER'S THEOREM

All the ground states in our phase diagram in Fig. 3 contain Fermi surfaces. In Fig. 5 we presented the evolution of the Fermi wavevectors of these Fermi surfaces in our mean-field calculation. In the present section we will discuss general constraints that must be satisfied by these Fermi wavevectors which are valid to all orders in the interactions. (Throughout this section, we shall be concerned only with $T = 0$.)

We will base our arguments upon the existence of the Luttinger-Ward functional[18] $\Phi_{\rm LW}$, satisfying

$$\Sigma = \left. \frac{\delta \Phi_{\rm LW}[G']}{\delta G'} \right|_{G'=G}, \tag{5.1}$$

where $G'$ is a dummy variable, $G$ is the actual full (thermal) Green function and $\Sigma$ is the full self-energy. (Throughout this section, we will mostly be concerned with the full Green functions, which we shall denote with the symbol $G$. When we make reference to the free Green function, this will be denoted $G_0$.)

Following Ref. 19, it possible to construct the Luttinger-Ward functional non-perturbatively, starting

from the partition function $Z$ of the system. It can be shown straightforwardly that, treating the Green function as a matrix in its momentum (and frequency) indices, any unitary transformation of the free Green function, $G_0 \to UG_0U^{-1}$, that leaves $Z$ invariant also leaves $\Phi_{\rm LW}$ invariant.

A standard proof of Luttinger's theorem[20] for a system of interacting fermions makes use of the invariance of $Z$ under a shift in the frequency appearing in the free propagator, $\omega \to \omega + \alpha$. In our case $\Phi_{\rm LW}$ is a functional of the three Green functions, one for each species, and $Z$ is invariant under a simultaneous shift in two of the three frequencies, *i.e.*

$$\begin{aligned} &\Phi_{\rm LW}[G^\psi(i\nu_1), G^f(i\nu_2), G^b(i\omega)] \\ &= \Phi_{\rm LW}[G^\psi(i\nu_1), G^f(i\nu_2 - i\alpha), G^b(i\omega + i\alpha)] \\ &= \Phi_{\rm LW}[G^\psi(i\nu_1 + i\beta), G^f(i\nu_2), G^b(i\omega + i\beta)] \end{aligned} \quad (5.2)$$

for any $\alpha$ and $\beta$.

To proceed further, it is useful to set $\mu^b = \mu^\psi - \mu^f$ and consider derivatives of the grand energy with respect to $\mu^f$ and $\mu^\psi$. The derivative with respect to $\mu^f$ yields

$$\left\langle f^\dagger f \right\rangle - \left\langle b^\dagger b \right\rangle = N_f - N_b \; . \quad (5.3)$$

Each term on the left-hand side can be rewritten in terms of the full Green functions, giving

$$N_f - N_b = -\int \frac{d^3k\, d\omega}{(2\pi)^4} e^{i\omega 0^+} \left[ G_k^f(i\omega) + G_k^b(i\omega) \right] \; . \quad (5.4)$$

(The change of sign of the $f$ term results from the anticommutation of fermion operators.)

From now on the manipulations are standard.[20] We make use of the identity

$$G(i\omega) = iG(i\omega)\frac{\partial}{\partial\omega}\Sigma(i\omega) - \frac{\partial}{\partial\omega}\ln G(i\omega) \; , \quad (5.5)$$

which results from the Dyson equation. The first equation of (5.2) gives, together with (5.1),

$$\int \frac{d^3k\, d\omega}{(2\pi)^4} \left[ \Sigma_k^b(i\omega)\frac{\partial}{\partial\omega} G_k^b(i\omega) + \Sigma_k^f(i\omega)\frac{\partial}{\partial\omega} G_k^f(i\omega) \right] = 0 \; . \quad (5.6)$$

Combining these two with (5.4) and integrating by parts gives

$$N_f - N_b = i\int \frac{d^3k\, d\omega}{(2\pi)^4} e^{i\omega 0^+} \frac{\partial}{\partial\omega} \left[ \ln G_k^f(i\omega) + \ln G_k^b(i\omega) \right] \quad (5.7)$$

(with the boundary terms vanishing because $G(i\omega) \sim 1/|\omega|$ for $|\omega| \to \infty$).

The integral over $\omega$ can be treated as a contour integration and closed above, due to the factor $e^{i\omega 0^+}$. Changing the integration variable to $z = i\omega$ replaces this by an integral surrounding the left half-plane. Since both of the full Green functions $G_k^{b,f}(z)$ have all their non-analyticities and zeroes on the line of real $z$, we can write this as

$$N_f - N_b = i\int \frac{d^3k}{(2\pi)^3} \int_{-\infty}^{0} \frac{dz}{2\pi}\frac{\partial}{\partial z} \left[ \ln G_k^f(z + i0^+) + \ln G_k^b(z + i0^+) - \ln G_k^f(z + i0^-) - \ln G_k^b(z + i0^-) \right] \; . \quad (5.8)$$

The integral of $z$ can be performed trivially to give

$$N_f - N_b = i\int \frac{d^3k}{(2\pi)^4} \left[ \ln \frac{G_k^f(i0^+)}{G_k^f(i0^-)} + \ln \frac{G_k^b(i0^+)}{G_k^b(i0^-)} \right] \; . \quad (5.9)$$

Using the analyticity properties of the Green functions, this gives

$$N_f - N_b = \int \frac{d^3k}{(2\pi)^3} \left[ \Theta(-\xi_k^f + \Sigma_k'^f) + \Theta(-\xi_k^b + \Sigma_k'^b) \right] \; , \quad (5.10)$$

where $\Theta$ is the unit step function and $\Sigma'$ is the real part of the self-energy evaluated for $\omega = 0$.

First, we consider the phase with no BEC. Here there are necessarily two Fermi surfaces, and, as we will now show, the volumes of the two Fermi surfaces are separately constrained, independently of the interactions.

By definition, the absence of a BEC requires that there be no bosonic quasiparticle excitations at or above the chemical potential, so that the second term in the brackets in (5.10) vanishes. (Note that this does not imply that $\left\langle b^\dagger b \right\rangle = 0$, which is not the case beyond mean-field order.) This leaves the statement of Luttinger's theorem for this case:

$$N_f - N_b = \int \frac{d^3k}{(2\pi)^3} \Theta(-\xi_k^f + \Sigma_k'^f) \; . \quad (5.11)$$

The right-hand side of this expression is interpreted as the (reciprocal-space) volume of the atomic Fermi surface.

A similar result follows by taking the derivative of the grand energy with respect to $\mu^\psi$, which gives

$$\left\langle \psi^\dagger \psi \right\rangle + \left\langle b^\dagger b \right\rangle = N_b \; . \quad (5.12)$$

Going through the same manipulations as above leads to

$$N_b = \int \frac{d^3k}{(2\pi)^3} \left[ \Theta(-\xi_k^\psi + \Sigma_k'^\psi) - \Theta(-\xi_k^b + \Sigma_k'^b) \right] \; , \quad (5.13)$$

corresponding to (5.10). Since we are in the phase with no BEC, this gives

$$N_b = \int \frac{d^3k}{(2\pi)^3}\Theta(-\xi_k^\psi + \Sigma_k'^\psi) \; . \tag{5.14}$$

We have therefore proved that there are two statements of Luttinger's theorem in the phase with two Fermi surfaces and no BEC. One, (5.11), states that the volume of the atomic Fermi surface is fixed by the difference in the numbers of atomic fermions and bosons, while the other, (5.14), states that the volume of the molecular Fermi surface is fixed by the total number of bosonic atoms.

Now let us extend our considerations to the phases with a BEC. In Fig. 3 we observe that these phases may have either one or two Fermi surfaces. Here we show that Luttinger's theorem only demands that the total volume enclosed within *both* Fermi surfaces is determined by $N_f$; the volumes of the two Fermi surfaces (if present) are not constrained separately.

In the presence of a BEC, it is no longer the case that the second term in the brackets vanishes in (5.10) and (5.13). Instead, if we add these two equations, we arrive at

$$N_f = \int \frac{d^3k}{(2\pi)^3}\Theta(-\xi_k^f + \Sigma_k'^f) + \int \frac{d^3k}{(2\pi)^3}\Theta(-\xi_k^\psi + \Sigma_k'^\psi) \; . \tag{5.15}$$

The two terms in this expression give the volumes of the two Fermi surfaces. We see that their sum is constrained to equal the number of fermionic atoms.

### A. Multicritical point

A simple application of our statements of Luttinger's theorem can be used to show that the multicritical point, where the three phases meet in Fig. 3 (and where four phases meet in Fig. 6), occurs at precisely $N_b = N_f$.

Firstly, according to (5.11), the volume of the atomic Fermi surface is given by $N_f - N_b$, as long as there is no BEC. This is therefore the case on the line dividing the phases with and without condensates, since the condensate vanishes as this line is approached from below. Secondly, the line that divides the regions with one and two Fermi surfaces is the point where the atomic Fermi surface vanishes. Where the two lines meet, we see both that (5.11) is satisfied and that its right-hand side vanishes. We therefore have $N_b = N_f$.

## VI. QUANTUM PHASE TRANSITIONS

We now present an alternative analysis using the language of field theory. In Section VI A, we reproduce the result that (4.7) determines the presence of the condensate. Then, in Section VI B, we determine the boson propagator near the BEC depletion transition. In Section VI C, we describe the critical field theories for the various transitions.

The dimensionless Euclidean action corresponding to the Hamiltonian (2.4) is

$$\begin{aligned}\mathcal{S} \;=\; & \frac{1}{\beta}\sum_q \bar f_q \Xi_q^f f_q + \frac{1}{\beta}\sum_p \bar b_p \Xi_p^b b_p + \frac{1}{\beta}\sum_q \bar\psi_q \Xi_q^\psi \psi_q \\ & - \frac{g}{\beta^2}\sum_{p,q}\left(\bar\psi_q f_{q-p} b_p + \bar b_p \bar f_{q-p}\psi_p\right) \; . \end{aligned} \tag{6.1}$$

The symbol $p$ stands for $k$ and $\omega_n$, and likewise $q$ for $\ell$ and $\nu_m$, where the Matsubara frequencies $\omega_n$ ($\nu_m$) are even (odd). The summations over $p$ ($q$) represent sums over $\omega_n$ ($\nu_m$) and integrals over the momentum $k$ ($\ell$). We have also defined

$$\Xi_p = (G_p)^{-1} = -i\omega_n + \xi_k \; , \tag{6.2}$$

the inverse of the free Green function, $G_p$, and similarly $\Xi_q$. (In this section and the following, we will use the symbol $G$ to denote the free Green function, contrary to the notation of Section V.)

We have omitted from the action the coupling term between pairs of bosons, since we will be interested in the region near the phase transition, where this term is not important.

Integrating out both of the fermions and expanding the resulting coupling term to quadratic order in $b$ and $\bar b$, we find that the effective action for the bosons is

$$\mathcal{S}_{\rm eff}^{(2)}[b,\bar b] = \frac{1}{\beta}\sum_p \bar b_p \Xi_p^b b_p + \frac{g^2}{\beta^2}\sum_{p,q} G_q^f G_{q+p}^\psi \bar b_p b_p \; . \tag{6.3}$$

### A. Mean-field approximation

By replacing $b$ by a real constant $\varphi$, we should arrive at the results of Section IV. In this approximation, we have

$$\mathcal{S}_{\rm eff}^{(2)}[b,\bar b] = -\mu^b\varphi^2 + \frac{g^2}{\beta}\varphi^2\sum_q G_q^f G_q^\psi \; , \tag{6.4}$$

so that the coefficient is

$$\Delta = -\mu^b + g^2\int\frac{d^d\ell}{(2\pi)^d}\frac{1}{\beta}\sum_{\nu_m} G_\ell^f(i\nu_m)\, G_\ell^\psi(i\nu_m) \; . \tag{6.5}$$

The phase transition will occur when the coefficient $\Delta$ vanishes.

We can represent (6.5) by

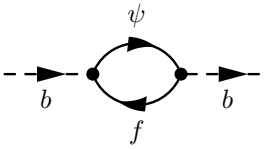


, (6.6)

which appears as a self-energy diagram in the boson propagator, drawn as a dashed line. (The two solid lines represent fermion propagators.)

The Matsubara sum can be performed by replacing it by a contour integration, giving

$$\Delta = -\mu^b + g^2 \int \frac{d^d\ell}{(2\pi)^d} \frac{n_{\rm F}(\xi_\ell^f) - n_{\rm F}(\xi_\ell^\psi)}{\xi_\ell^f - \xi_\ell^\psi} \ , \qquad (6.7)$$

in agreement with (4.7).

### B. Boson propagator

By retaining the frequency dependence of the boson field, but again keeping only terms quadratic in $b$ and $\bar{b}$, we can determine the form of the long-wavelength, low-frequency excitations.

The effective boson propagator is, from (6.3), the reciprocal of

$$\begin{aligned} \widetilde{\Xi}_k^b(i\omega_n) \ &\equiv \ \widetilde{\Xi}_p^b \ \equiv \ \Xi_p^b + \frac{g^2}{\beta} \sum_q G_q^f G_{q+p}^\psi \qquad (6.8) \\ &= \ -i\omega_n + \xi_k^b + g^2 \int \frac{d^d\ell}{(2\pi)^d} \times \\ &\quad \frac{1}{\beta} \sum_{\nu_m} \frac{1}{-i\nu_m + \xi_\ell^f} \frac{1}{-i(\nu_m + \omega_n) + \xi_{\ell+k}^\psi} \ , \end{aligned}$$

which replaces (6.5). For $k = 0$, this gives

$$\widetilde{\Xi}_0^b(i\omega_n) = -i\omega_n - \mu^b + g^2 \int \frac{d^d\ell}{(2\pi)^d} \frac{n_{\rm F}(\xi_\ell^f) - n_{\rm F}(\xi_\ell^\psi)}{\xi_\ell^f - \xi_\ell^\psi + i\omega_n} \ , \qquad (6.9)$$

where the result

$$n_{\rm F}(a - i\omega_n) = n_{\rm F}(a) \ , \qquad (6.10)$$

for $\omega_n$ a boson Matsubara frequency, has been used. For small $\omega_n$, we can expand to give

$$\begin{aligned} \widetilde{\Xi}_0^b(i\omega_n) \ &\simeq \ \Delta - i\omega_n \left[ 1 - g^2 \int \frac{d^d\ell}{(2\pi)^d} \frac{n_{\rm F}(\xi_\ell^f) - n_{\rm F}(\xi_\ell^\psi)}{\left(\xi_\ell^f - \xi_\ell^\psi\right)^2} \right] \\ &\quad - \omega_n^2 g^2 \int \frac{d^d\ell}{(2\pi)^d} \frac{n_{\rm F}(\xi_\ell^f) - n_{\rm F}(\xi_\ell^\psi)}{\left(\xi_\ell^f - \xi_\ell^\psi\right)^3} \ . \qquad (6.11) \end{aligned}$$

(Note that, as required, the coefficient of $\omega_n^2$ is in fact positive.)

The effective boson propagator (for $k = 0$) is then

$$\widetilde{G}_0^b(i\omega_n) = \frac{\mathcal{Z}}{-i\omega_n + \tilde{\xi}_0^b(\omega_n)} \ , \qquad (6.12)$$

with

$$\mathcal{Z} = \left[ 1 - g^2 \int \frac{d^d\ell}{(2\pi)^d} \frac{n_{\rm F}(\xi_\ell^f) - n_{\rm F}(\xi_\ell^\psi)}{\left(\xi_\ell^f - \xi_\ell^\psi\right)^2} \right]^{-1} \ , \qquad (6.13)$$

and

$$\tilde{\xi}_0^b(\omega_n) = \mathcal{Z} \left[ \Delta - \omega_n^2 g^2 \int \frac{d^d\ell}{(2\pi)^d} \frac{n_{\rm F}(\xi_\ell^f) - n_{\rm F}(\xi_\ell^\psi)}{\left(\xi_\ell^f - \xi_\ell^\psi\right)^3} \right] \ . \qquad (6.14)$$

The integrals in the expressions for both $\mathcal{Z}$ and $\tilde{\xi}_0^b(\omega_n)$ diverge at zero temperature if $N_f = 2N_b$ so that the two Fermi wavenumbers coincide. For any other parameters the integrals are finite, and the effective propagator has the form (6.12). As we discuss in the following subsection, this distinction leads to different field theories for the BEC depletion quantum transition for these cases.

### C. Critical field theories

First, we consider the BEC depletion quantum transition. This is the transition between the 2 FS + BEC phase and the 2 FS, no BEC phase in Fig. 3. The same theory also applies to the transition between the 1 FS + BEC phase and the 1 FS, no BEC phase in Fig. 6. The low momentum modes of the $b$ boson field clearly constitute an order parameter for this transition. The effective action for the renormalized $b$ field near the critical point can be derived by integrating out the fermionic degrees of freedom, as already outlined in Section VI B.

For $N_f \neq 2N_b$, the integration of the fermionic excitations is entirely free of infrared singularities: the differences in the two Fermi wavevectors implies that there are no low momentum fermionic particle-hole excitations at low energies. The resulting action for $b$ contains only terms which are analytic in frequency and momentum, and has the following familiar form:

$$\begin{aligned} \mathcal{S}_c[b] \ &= \ \int d^3r \int d\tau \left[ b^\dagger \frac{\partial b}{\partial \tau} - \frac{1}{2\tilde{m}^b} b^\dagger \nabla^2 b + s|b|^2 \right. \\ &\quad \left. + \frac{u}{2}|b|^4 \right] \qquad (6.15) \end{aligned}$$

Note that the $b$ field has been rescaled by a factor $\sqrt{\mathcal{Z}}$ from the $b$ field in Section VI B and that its mass has been replaced by the renormalized mass $\tilde{m}^b$. The action $\mathcal{S}_c[b]$ describes a quantum phase transition with dynamic exponent $z = 2$ driven by tuning the coupling $s$. This transition has been discussed previously in Ref. 12 and in Chapter 11 of Ref. 13. The upper critical dimension is $d = 2$, above which the quartic coupling $u$ is formally irrelevant. Nevertheless, the coupling $u$ is important for the $T > 0$ crossovers in the vicinity of the quantum critical point: these are as presented in Ref. 13.

For $N_f = 2N_b$, there are low energy fermionic particle-hole excitations at zero momentum, and so the above procedure has to be reconsidered. Now there are non-analytic terms in the effective action for $b$, but these have a structure similar to that found by Hertz[21] for the onset of ferromagnetism in a Fermi liquid. Evaluating (6.8) for

this case following Hertz, we now find the effective action

$$\mathcal{S}_c[b] = \int d^3k \int d\omega |b(k,\omega)|^2 \left[k^2 + c\frac{|\omega|}{k}\right] + \int d^3r \int d\tau \left[s|b|^2 + \frac{u}{2}|b|^4\right]. \quad (6.16)$$

The bare $-i\omega$ term in the boson propagator is not included above because it is less relevant than the non-analytic term generated from the Fermi surface excitations. The critical properties of the $z = 3$ critical theory in Eq. (6.16) have been described earlier by Hertz, and the $T > 0$ crossovers by Millis[22] (see also Chapter 12 of Ref. 13).

Next, we consider the critical theory of the 2 FS + BEC to 1 FS + BEC transition in Fig. 3. The same theory also applies to the 2 FS, no BEC to 1 FS, no BEC transition in Fig. 6. Here, a Fermi surface disappears as its Fermi wavevector vanishes. The critical theory is then the $z = 2$ dilute Fermi gas theory already discussed in Chapter 11 of Ref. 13. All interactions are irrelevant for the critical properties, and the quantum-critical crossovers are merely those of a free Fermi gas.

Finally, consider the multi-critical point, noted in Section V A, where all phases in Fig. 3 and Fig. 6 meet. Here, both the $b$ bosons and the $f$ fermions are critical. The critical theory is merely the direct sum of the $z = 2$ dilute Bose and Fermi theories mentioned above. All interactions between the critical $f$ and $b$ modes are formally irrelevant in three spatial dimensions.

## VII. GAUSSIAN CORRECTIONS

In order to test the validity of the approximations made, we shall calculate two different corrections to the mean-field results of the preceding sections. First, in this section, we find the corrections to the grand free energy $\Phi$ to order $g^2$. These will result in corrections to the expressions found in Section IV B relating the chemical potentials to the particle numbers. Subsequently, in Section VIII, we will find a new expression for $\Delta$ by replacing the mean-field theory with a low-density approximation.

In the remainder of this section, we will use $\widetilde{\Xi}^b$ from (6.8) to determine the corrections to the grand free energy $\Phi$. We will show that these are negligible, provided that the dimensionless coupling $\gamma^2/T_0$ is sufficiently small. We therefore require a narrow Feshbach resonance for the results to be quantitatively accurate.

By integrating the effective action over the boson field, we arrive at an expression for the partition function including Gaussian corrections,

$$Z^{(2)} = \frac{(\det \Xi^f)(\det \Xi^\psi)}{(\det \widetilde{\Xi}^b)} . \quad (7.1)$$

The grand free energy is then given by

$$\Phi = \Phi_0^f + \Phi_0^\psi + \frac{1}{\beta}\sum_p \ln\left(\Xi_p^b + \frac{g^2}{\beta}\sum_q G_q^f G_{q+p}^\psi\right) , \quad (7.2)$$

using (6.8), where

$$\Phi_0^x = \pm\frac{1}{\beta}\sum_q \ln \Xi_q^x \quad (7.3)$$

is the grand free energy for the species $x$ in the absence of coupling. [The plus (minus) sign applies to bosons (fermions).]

Taking a factor of $\Xi_p^b$ out of the logarithm gives $\Phi_0^b$, so that the correction to $\Phi$ is

$$\Phi - \Phi_0 = \frac{1}{\beta}\sum_p \ln\left(1 + \frac{g^2}{\beta}\sum_q G_q^f G_{q+p}^\psi G_p^b\right) . \quad (7.4)$$

This is the full expression for the Gaussian corrections; to estimate the size of these corrections, we will calculate the result to order $g^2$. Dropping terms of higher order gives a correction to the free energy $\Phi$ of

$$\Delta\Phi = \frac{g^2}{\beta^2}\sum_{p,q} G_q^f G_{q+p}^\psi G_p^b , \quad (7.5)$$

which can be represented diagrammatically as

$\Delta\Phi$ =

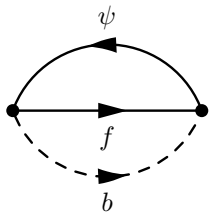


. (7.6)

Reinstating explicit momentum integrals and frequency sums, we have

$$\Delta\Phi = \frac{g^2}{\beta^2}\sum_{\omega_n,\nu_m}\int \frac{d^dk}{(2\pi)^d}\frac{d^d\ell}{(2\pi)^d} G^b(\omega_n,k)\, G^f(\nu_m,\ell)\, G^\psi(\nu_m+\omega_n,\ell+k) \quad (7.7)$$

Both Matsubara sums can be performed using contour integration, to give

$$\Delta\Phi = g^2 \int \frac{d^dk}{(2\pi)^d}\int \frac{d^d\ell}{(2\pi)^d} \frac{\left[n_{\rm F}(\xi^f_{\ell-k}) - n_{\rm F}(\xi^\psi_\ell)\right]\left[n_{\rm B}(\xi^b_k) - n_{\rm B}(\xi^\psi_\ell - \xi^f_{\ell-k})\right]}{\xi^b_k + \xi^f_{\ell-k} - \xi^\psi_\ell} , \quad (7.8)$$

after a change of variables, $\ell \to \ell - k$.

### A. Renormalization of the detuning

As it stands, the integral over $k$ is in fact divergent. As $|k|$ tends to infinity (with $|\ell|$ finite), the second Bose factor, $n_{\rm B}(\xi^{\psi}_{\ell} - \xi^{f}_{\ell-k})$, tends to $-1$. In the first bracket, $n_{\rm F}(\xi^{\psi}_{\ell})$ remains finite, so the integrand tends to $\sim 1/k^2$ and the integral over $k$ is linearly divergent.

This divergence can be understood by considering the self-energy diagram

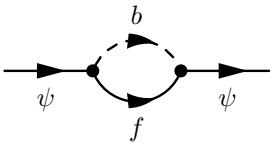


(7.9)

which gives a correction to the detuning $\nu$ linear in the cut-off momentum,

$$\nu = \nu_0 - g^2 \int \frac{d^d k}{(2\pi)^d} \frac{2m^f m^b}{m^{\psi}} \frac{1}{k^2} \, , \tag{7.10}$$

where $\nu_0$ is the 'bare' detuning that appears explicitly in the action.

We use this expression to write $\nu_0$, which appears within $\Xi^{\psi}$ in (7.1), in terms of $\nu$, and then keep terms only of order $g^2$. The renormalized expression for $\Delta\Phi$ is then given by

$$\Delta\Phi = g^2 \int \frac{d^d k}{(2\pi)^d} \int \frac{d^d \ell}{(2\pi)^d} \left\{ \frac{\left[ n_{\rm F}(\xi^{f}_{\ell-k}) - n_{\rm F}(\xi^{\psi}_{\ell}) \right] \left[ n_{\rm B}(\xi^{b}_{k}) - n_{\rm B}(\xi^{\psi}_{\ell} - \xi^{f}_{\ell-k}) \right]}{\xi^{b}_{k} + \xi^{f}_{\ell-k} - \xi^{\psi}_{\ell}} + \frac{2m^f m^b}{m^{\psi}} \frac{n_{\rm F}(\xi^{\psi}_{\ell})}{k^2} \right\} \, , \tag{7.11}$$

where the dispersion relation $\xi^{\psi}$ now involves the renormalized (physical) detuning $\nu$. (We have retained the same symbols for the new, renormalized quantities.)

This expression can be simplified somewhat by performing a further change of variable, taking $k \to k + (m^b/m^{\psi})\ell$, and also making use of the result

$$n_{\rm F}(x) n_{\rm B}(y-x) + n_{\rm F}(y) n_{\rm B}(x-y) = -n_{\rm F}(x) n_{\rm F}(y) \, . \tag{7.12}$$

We have finally

$$\Delta\Phi \; = g^2 \int \frac{d^d k}{(2\pi)^d} \int \frac{d^d \ell}{(2\pi)^d} \frac{1}{\frac{m^{\psi}}{2m^f m^b} k^2 - \nu} \left[ n_{\rm F}(\xi^f) n_{\rm B}(\xi^b) - n_{\rm F}(\xi^{\psi}) n_{\rm B}(\xi^b) + n_{\rm F}(\xi^f) n_{\rm F}(\xi^{\psi}) - n_{\rm F}(\xi^{\psi}) \frac{2m^f m^b}{m^{\psi}} \frac{\nu}{k^2} \right] \, , \tag{7.13}$$

in which the energies $\xi^{\psi}$, $\xi^f$ and $\xi^b$ should be evaluated at the following momenta:

$$\xi^{\psi} \; \equiv \; \xi^{\psi}(\ell) \tag{7.14}$$

$$\xi^{f} \; \equiv \; \xi^{f}(k - \tfrac{m^f}{m^{\psi}}\ell) \tag{7.15}$$

$$\xi^{b} \; \equiv \; \xi^{b}(k + \tfrac{m^b}{m^{\psi}}\ell) \, . \tag{7.16}$$

Note that there is no singularity in the integral over $k$ in (7.13), since the numerator also vanishes at the point where

$$|k| = \sqrt{\nu \frac{2m^f m^b}{m^{\psi}}} \tag{7.17}$$

(for $\nu > 0$).

The expression for $\Delta\Phi$ must be differentiated with respect to the chemical potentials to give the correction to the number of each species of particle. The resulting integral can then be performed numerically.

The results of such a calculation are shown in Fig. 7, where we plot the corrections to the particle numbers. These have been divided by the total numbers evaluated using the results of Section IV B. The atomic masses have been taken to be equal, as in Fig. 1, and, at each temperature value, the detuning takes on its critical value.

We have taken for the dimensionless coupling $\gamma^2/T_0 = 2.5 \times 10^{-4}$, as in Fig. 1, so that this corresponds to a narrow Feshbach resonance. Since the correction everywhere is less than 5% of the total numbers, we expect that the mean-field results provide a good approximation for this case. The magnitude of the correction scales with $g^2 \propto \gamma$, so that the quantitative predictions become less reliable for a broader resonance.

## VIII. LOW-DENSITY APPROXIMATION

In this section, we develop a low-density approximation involving all orders in the coupling $g$.

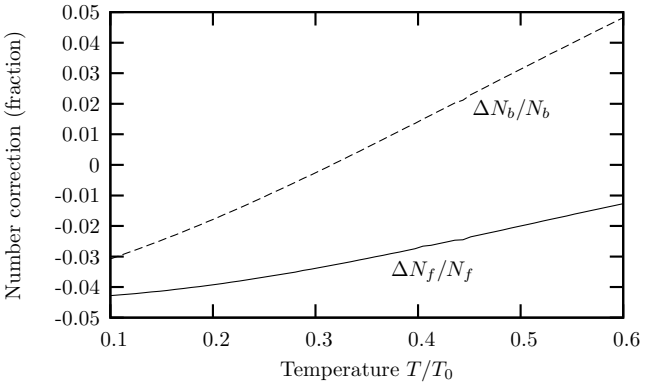


FIG. 7: Two-loop corrections to particle numbers, shown as a fraction of the total particle numbers to lowest order. The masses of the particles and their total numbers are the same as in Fig. 1, $N_f/N_b = 1.11$. The dimensionless coupling is $\gamma^2/T_0 = 2.5 \times 10^{-4}$. At each temperature, the corrections have been evaluated taking the detuning at its critical value, from Fig. 1.

### A. Diagrammatic description

In the mean-field approximation, we have included in the boson self-energy such diagrams as

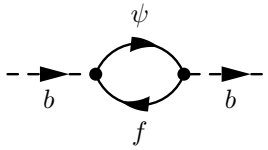


(8.1)

whose amplitude is proportional to the density of atoms in the system. (A fermionic atom must be present in the system initially, in order to couple with the boson.) Diagrams involving further loops with bosonic or fermionic atoms, such as

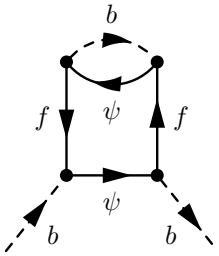


(8.2)

are proportional to higher powers of the density.

There is, however, a correction to the molecular propagator of order zero in density coming from the process shown in (7.9), which can take place in the vacuum. To make a consistent low-density approximation, we must therefore correct the molecular propagator using a Dyson equation

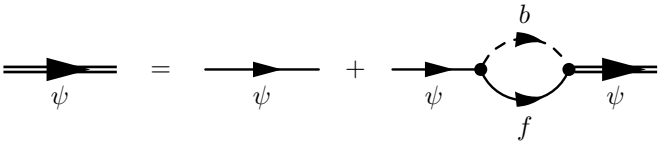


(8.3)

where only the term in the bubble diagram (7.9) of order zero in density is to be included.

The boson self-energy diagram

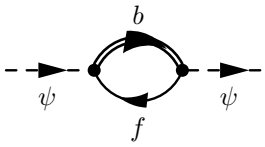


(8.4)

should now be used to give a low-density approximation for the phase transition.

### B. Calculations

The Dyson equation (8.3) gives the relation between the reciprocals of the bare and full Green functions

$$\widetilde{\Xi}_q^\psi = \Xi_q^\psi - \frac{g^2}{\beta}\sum_p G_{q-p}^f G_p^b \; ; \tag{8.5}$$

compare (6.8). [The sign difference results from the fermion loop in (6.6).]

Including only corrections to order zero in density, by dropping the Bose- Einstein and Fermi-Dirac factors, gives

$$\widetilde{\Xi}_q^\psi = \Xi_q^\psi - g^2 \int \frac{d^d k}{(2\pi)^d}\left(\frac{1}{\xi_k^b + \xi_{\ell-k}^f - i\nu_m} - \frac{2m^f m^b}{m^\psi k^2}\right) , \tag{8.6}$$

where $q \equiv (\ell, \nu_m)$. (The second term in the parentheses comes from renormalizing the detuning $\nu$, as in Section VII A above.) The integral can be performed analytically, to give

$$\widetilde{\Xi}_q^\psi = \Xi_q^\psi + 2\gamma\sqrt{\xi_\ell^\psi - \nu - i\nu_m} \; , \tag{8.7}$$

where $\gamma$, defined in (2.6), has been used.

This function can be continued to one that is analytic everywhere except along the real axis, by replacing $i\nu_m$ by $z$. In terms of $z$, the full Green function is

$$\widetilde{G}_\ell^\psi(z) = \frac{-1}{z - \xi_\ell^\psi - 2\gamma\sqrt{\xi_\ell^\psi - \nu - z}} \, . \tag{8.8}$$

Along the real axis, the square root has a branch cut for $z > \xi_\ell^\psi - \nu$ which corresponds to the continuum of free-atom excitations. For $\nu < 0$, $\widetilde{G}^\psi$ has a single pole at the real value

$$z_0 = \xi_\ell^\psi - 2\gamma^2\left(1 - \sqrt{1 - \tfrac{\nu}{\gamma^2}}\right) \; , \tag{8.9}$$

corresponding to the renormalized molecule. For $\nu > 0$, there are no poles, since the molecule has a finite lifetime, decaying into two atoms.

### C. Spectral representation

These analytical properties are best summarized using the spectral representation for $\widetilde{G}^{\psi}$,

$$\widetilde{G}^{\psi}_{\ell}(z) = \int_{-\infty}^{\infty} dx\, \frac{\rho^{\psi}_{\ell}(x)}{x - z}\ . \tag{8.10}$$

The 'spectral density' is given by

$$\rho^{\psi}_{\ell}(x) = \Theta(x - \xi^{\psi}_{\ell} + \nu)\, \frac{2\gamma}{\pi}\, \frac{\sqrt{x - \xi^{\psi}_{\ell} + \nu}}{\left(x - \xi^{\psi}_{\ell}\right)^2 + 4\gamma^2\left(x - \xi^{\psi}_{\ell} + \nu\right)} + \Theta(-\nu)\frac{\sqrt{1 - \frac{\nu}{\gamma^2}} - 1}{\sqrt{1 - \frac{\nu}{\gamma^2}}}\, \delta\Big(x - \xi^{\psi}_{\ell} - 2\gamma^2\left(\sqrt{1 - \tfrac{\nu}{\gamma^2}} - 1\right)\Big)\ , \tag{8.11}$$

where $\Theta$ is the unit step function and $\delta$ is the Dirac delta function.

#### 1. Weak-coupling limit

It should be noted that, in the limit of small coupling, $\gamma \to 0$, the first term of (8.11) involves the Lorentzian representation of the Dirac delta function,

$$\lim_{\varepsilon \to 0} \frac{\varepsilon}{\pi(t^2 + \varepsilon^2)} = \delta(t)\ . \tag{8.12}$$

For $\gamma$ small enough, the first term of (8.11) has weight only near $x = \xi^{\psi}_{\ell}$, where $x - \xi^{\psi}_{\ell} + \nu$ can be replaced by $\nu$. The limit of vanishing $\gamma$ is therefore given by

$$\lim_{\gamma \to 0} \frac{2\gamma}{\pi}\, \frac{\sqrt{x - \xi^{\psi}_{\ell} + \nu}}{\left(x - \xi^{\psi}_{\ell}\right)^2 + 4\gamma^2\left(x - \xi^{\psi}_{\ell} + \nu\right)} = \delta(x - \xi^{\psi}_{\ell})\ , \tag{8.13}$$

so that the spectral density becomes, in this limit,

$$\begin{aligned} \rho^{\psi}_{\ell}(x) \ &\to\ \Theta(x - \xi^{\psi}_{\ell} + \nu)\delta(x - \xi^{\psi}_{\ell}) + \Theta(-\nu)\delta(x - \xi^{\psi}_{\ell}) \\ &=\ \delta(x - \xi^{\psi}_{\ell})\ , \end{aligned} \tag{8.14}$$

which is precisely the result for the bare molecule, used in Section VI.

### D. Effective action for bosons

Using the modified spectral density for the molecule, (8.11), we can compute the quadratic term in the effective action for the boson field. Following Section VI A, the modified coefficient is

$$\widetilde{\Delta} = -\mu^b + g^2 \int \frac{d^d\ell}{(2\pi)^d}\, \frac{1}{\beta} \sum_{\nu_m} G^f_{\ell}(i\nu_m)\, \widetilde{G}^{\psi}_{\ell}(i\nu_m)\ . \tag{8.15}$$

We can now use the spectral representation for both Green functions and then perform the Matsubara sum. Since the spectral density for the $f$ atom has the form

$$\rho^f_{\ell}(x) = \delta(x - \xi^f_{\ell})\ , \tag{8.16}$$

the low-density approximation to the discriminant is given by

$$\widetilde{\Delta} = -\mu^b + g^2 \int \frac{d^d\ell}{(2\pi)^d} \int_{-\infty}^{\infty} dx\, \rho^{\psi}_{\ell}(x) \frac{n_{\rm F}(x) - n_{\rm F}(\xi^f_{\ell})}{x - \xi^f_{\ell}}\ , \tag{8.17}$$

with $\rho^{\psi}_{\ell}(x)$ given by (8.11), above. This integral can be performed numerically.

Since $\widetilde{\Delta}$ provides a correction to $\Delta$, we must find some measure by which to determine the significance of this correction. A comparison with $\Delta$ is obviously not possible, since this vanishes everywhere along the mean-field curve in Fig. 1. Instead, we shall find a lowest-order correction to the critical detuning by evaluating

$$\delta\nu \equiv \left(\widetilde{\Delta} - \Delta\right) \Big/ \left(\frac{\partial \Delta}{\partial \nu}\right)_{\beta, N_f, N_b}\ . \tag{8.18}$$

(Finding the curve $\widetilde{\Delta} = 0$ exactly would require a much larger computational effort, since $\widetilde{\Delta}$ takes considerably more time to evaluate than $\Delta$. Instead, $\delta\nu$ provides the first step of a solution of $\widetilde{\Delta} = 0$ by Newton's iterative method.)

The partial derivative on the right-hand side of (8.18) is given by

$$\left(\frac{\partial\Delta}{\partial\nu}\right)_{N_f,N_b} = \left(\frac{\partial\Delta}{\partial\nu}\right)_{\mu^f,\mu^b} + \left(\frac{\partial\Delta}{\partial\mu^f}\right)_{\mu^b,\nu}\left(\frac{\partial\mu^f}{\partial\nu}\right)_{N_f,N_b} + \left(\frac{\partial\Delta}{\partial\mu^b}\right)_{\mu^f,\nu}\left(\frac{\partial\mu^b}{\partial\nu}\right)_{N_f,N_b} , \tag{8.19}$$

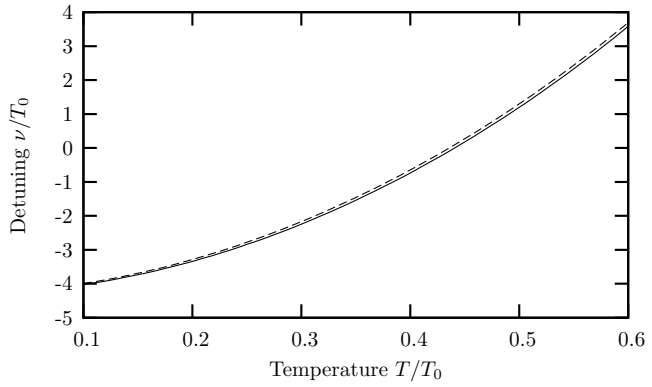


FIG. 8: The phase boundary, without (solid line) and with (dashed line) the correction to the detuning of Section VIII. The solid line is the phase boundary as in Fig. 1, using the same parameters (and dimensionless coupling $\gamma^2/T_0 = 2.5\times10^{-4}$). The dashed line includes the correction $\delta\nu$, from (8.18), found using a low-density approximation. For clarity, this correction has been exaggerated by a factor of 3. Since the correction is negligible for these parameters, the mean-field results of Sections IV and VI are sufficient.

where all the derivatives are to be taken at constant $\beta$. To lowest order in the coupling, this can be replaced by

$$\left(\frac{\partial\Delta}{\partial\nu}\right)_{N_f,N_b} = \left(\frac{\partial\mu^b}{\partial\nu}\right)_{N_f,N_b} + \mathcal{O}\left(g^2\right) , \tag{8.20}$$

using (4.7). The quantity on the right-hand side is the increase in the boson chemical potential needed to compensate an increase in the detuning, and keep the particle numbers unchanged. This can be evaluated using the expressions given in Section IV B.

The results of such a calculation are shown in Fig. 8. The solid line is the phase boundary shown in Fig. 1, using the same parameters. The dashed line is the same curve with the quantity $\delta\nu$ from (8.18) added. (For clarity, we have multiplied $\delta\nu$ by a factor of 3.) The small magnitude of the correction suggests that the results presented in Sections IV and VI are valid, for the parameters chosen. In this case, it is therefore unnecessary to use a low-density approximation; the mean-field result is sufficient.

## IX. CONCLUSIONS

From a theoretical perspective, the main contribution of this paper is a description of a quantum phase transition with an intimate connection to the Luttinger theorem. On one side of the transition (see Fig. 3), in the 2 FS, no BEC phase, there are 2 Fermi surfaces with a separate Luttinger theorem for each Fermi surface. Remarkably, one Fermi surface is constrained by the total number of *bosons* $N_b$, while the other is controlled by $N_f - N_b$, where $N_f$ is total number of fermions. These two Luttinger theorems are consequences of two number operators that commute with the Hamiltonian: the operator $f^\dagger f - b^\dagger b$ in Eq. (5.3), and the operator $f^\dagger f + \psi^\dagger\psi$ in Eq. (5.12). On the other side of the quantum critical point is the 2 FS + BEC phase. Here a Bose-Einstein condensate is present, and the condensate effectively thwarts one of the Luttinger constraints. The single remaining Luttinger theorem demands only that the total volume enclosed by both Fermi surfaces is constrained by $N_f$. We presented a theory for this transition, along with phase diagrams as a function of system parameters.

It is intriguing to note a connection between the above quantum phase transition and a seemingly disconnected, recent analysis of a quantum phase transition in a Kondo lattice model of the heavy fermion compounds.[23] This was a model of electrons occupying localized $f$ orbitals (the $f_\sigma$ electrons, where $\sigma$ is a spin index) interacting the itinerant electrons in the conduction band (the $c_\sigma$ electrons). A boson, $b$, was introduced to represent the hybridization between the orbitals. The connection between the Kondo lattice model and the model of the present paper now becomes clear once we identify the $c_\sigma$ electrons with the molecular fermionic state $\psi$, and the $f_\sigma$ electrons with the $f$ fermions. The Kondo lattice model also has two number constraints analogous to Eq. (5.3) and Eq. (5.12), with one crucial difference: the first constraint is local rather than global, and applies separately on each lattice site. With this mapping, the heavy Fermi liquid FL state of Ref. 23 can be identified with the 2 FS + BEC and the 1 FS + BEC phases. Further, the FL* phase of Ref. 23 is the analog of the present 2 FS, no BEC phase. The FL* phase also has two Luttinger theorems, one fixing the volume of the conduction band Fermi surface of electronic quasiparticles, and the other the volume of the 'spinon' Fermi surface. The presence of a local rather than a global constraint implies that there is an additional gauge force that affects the spinon Fermi surface and the quantum critical fluctuations of the Kondo lattice. Such gauge forces are absent in our present considerations of Bose-Fermi mixtures, but, apart from this absence, there is a remarkable similarity to the FL-FL* transition in Kondo lattice models.

On the experimental front, an obvious signature of the quantum phase transition in the Bose-Fermi mix-

tures is in the evolution of the Bose-Einstein condensate. It would be interesting to scan the detuning and look for the disappearance of the condensate fraction at the lowest temperatures. The corresponding "superfluid-normal" transition should also survive at $T > 0$, where its signatures are similar to the $\lambda$ transition in $^4$He.

A more dramatic, but experimentally less accessible, signature of the transition lies in the values of the Fermi wavevectors, as sketched in Fig. 5. Measuring the Fermi wavevectors would allow detection of a Fermi surface constrained by the number of bosons, and its eventual evolution across the transition to a Fermi surface constrained by the total number of fermions.

Finally, it should be noted that we have not addressed here the alternative of a paired state of fermions. Since we have dealt with spin-polarized fermions, $s$-wave pairing between the atoms is excluded, but $p$-wave pairing remains a possibility.[24] There is also the more novel possibility for pairing between the fermionic atoms $f$ and the molecules $\psi$, which could be favorable when the two Fermi wavenumbers are approximately equal. This would then lead to condensation of a composite boson comprised of two fermionic atoms and one bosonic atom. We intend to investigate this possibility further in future work.

**Acknowledgments**

We thank R. Hulet and W. V. Liu for valuable discussions. This research was supported by the National Science Foundation under grant DMR-0098226, and under grant DMR-0210790. S.S. was also supported by the John Simon Guggenheim Memorial Foundation.

## APPENDIX: STABILITY AGAINST PHASE SEPARATION

This section uses the mean-field results of Section IV. The temperature will be taken as zero throughout.

### 1. The compressibility matrix

To establish the stability of the system against separation into two coexisting fluids, we evaluate the compressibility matrix, defined by

$$K'_{\alpha\beta} = -\frac{\partial^2 \Phi}{\partial \mu^\alpha \partial \mu^\beta} \ , \tag{A.1}$$

for $\alpha, \beta \in \{f, b\}$.

We now define the (canonical) free energy $F(N_f, N_b)$ by a Legendre transformation,

$$F(N_f, N_b) = \Phi(\mu^f, \mu^\psi) + \mu^f N_f + \mu^b N_b \ , \tag{A.2}$$

where $N_f$ and $N_b$ are the total number of Fermi and Bose atoms, respectively. (Note that the full fermion and boson numbers, which are conserved by the Hamiltonian, are used.) The compressibility matrix $K'$ is then the inverse of the Hessian of $F$, so that complete stability against phase separation requires that $K'$ be positive semidefinite.

It is in fact easier to work with the matrix $K_{\alpha\beta}$, given by the same expression (A.1), but with $\alpha, \beta \in \{f, \psi\}$. This amounts to a simple (but not orthogonal) change of basis; it is sufficient (and necessary) for $K'$ to be positive semidefinite that $K$ be the same.

We begin with (4.4) and (4.5) and use (4.11) to determine the implicit dependence of $\varphi$ on the chemical potentials. We must then take second derivatives with respect to the two chemical potentials to find the compressibility matrix. In the presence of a condensate, this leads to an expression

$$K_{\alpha\beta} = K^{(0)}_{\alpha\beta} + \frac{r_\alpha r_\beta}{\tilde{\lambda}} \ , \tag{A.3}$$

where $K^{(0)}_{\alpha\beta}$ is the matrix of second derivatives, evaluated at fixed $\varphi$ and $r_\alpha$ is a function whose form will not concern us here.

The denominator of the second term is

$$\tilde{\lambda} = \lambda + g^4 \int_{k_0^F}^{k_0^\Psi} \frac{dn(k)}{W_k^3} - \tfrac{1}{2} g^4 \left( z^F + z^\Psi \right) \ , \tag{A.4}$$

where

$$z^x = \left. \frac{m^\psi m^f dn/dk}{k \left( \xi_k^f + \xi_k^\psi \right) \left( m^f \xi_k^f + m^\psi \xi_k^\psi \right)} \right|_{k = k_0^x} \tag{A.5}$$

and

$$W_k = \sqrt{\left( \xi_k^f - \xi_k^\psi \right)^2 + 4 g^2 \varphi^2} \ . \tag{A.6}$$

When $\tilde{\lambda}$ goes through zero, the determinant of $K$ diverges, so that the Hessian of $F$ becomes singular, signifying that one of its eigenvalues vanishes. This marks the onset of instability; we conclude that stability requires that $\tilde{\lambda} > 0$.

When there is no condensate, *i.e.* in the phase labeled '2 FS, no BEC' in Fig. 3, it is found that the system is always stable.

### 2. Physical interpretation

The obvious physical interpretation of $\tilde{\lambda}$ is that it represents the resultant interaction between the bosons, coming partly from the explicit term $\lambda$ in the Hamiltonian (2.4) and partly from the interaction induced by coupling to the fermions. This induced interaction can alternatively be found directly by continuing the expansion (6.3) to fourth order in $b$ and $\bar{b}$.

A resultant interaction of the form (A.4) is familiar from the case where the molecular degrees of freedom

are not included explicitly in the Hamiltonian.[25,26] This corresponds to our model for $\nu \gg 0$, when only virtual molecules are formed and the coupling term $\psi^\dagger f b$ in the Hamiltonian (2.4) can be replaced by a boson-fermion scattering of the form $f^\dagger b^\dagger b f$. The induced interaction then comes from the diagram

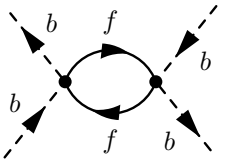


, (A.7)

which gives a term proportional to the density of states at the Fermi surface (at $T = 0$).

In this case, the induced interaction is always attractive, as can be shown by a simple physical argument. For experimentally accessible parameters, however, it is not strong enough to overcome the intrinsic repulsion between the bosons, so that the phase is stable.[25] In our notation, the boson-fermion scattering is suppressed by a factor of $1/\nu$, so that the induced interaction falls off as $1/\nu^2$. For $\nu \ll 0$, a similar picture is obtained, with the atomic and molecular fermions exchanging rôles.

In the case of intermediate $\nu$, the induced interaction is no longer so heavily suppressed, but it is also no longer the case that it is always attractive. The physical picture is clarified in this case by rewriting the action in (6.1) in terms of the fermions $F$ and $\Psi$ introduced in Section IV A. These fermions are defined so that there is no coupling term in the action linear in $\varphi = \langle b \rangle$; instead, the lowest order interactions have the form $\bar{F}\,\varphi^2\,F$ and $\bar{F}\,\varphi^4\,F$, and the same for $\Psi$. The former reproduces exactly the diagram (A.7) above, with $f$ replaced by $F$ and $\Psi$: physically this is a boson-fermion scattering inducing an attractive interaction between the bosons, as described above. This accounts for the final term in (A.4). Note that the exclusion principle requires the momenta of the two fermion lines to be exactly at the Fermi surface, leading to $z^x$ being evaluated at $k_0^x$.

The term $\bar{F}\,\varphi^4\,F$ produces the diagram

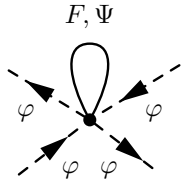


(A.8)

which also represents an induced boson-boson interaction and accounts for the integral in (A.4). Since $W_k \geq 0$, it is always repulsive and represents the fact that the fermion energy is lowered by a uniform distribution of bosons.

### 3. Results

The sign of the resultant interaction $\tilde{\lambda}$ must be calculated numerically to determine whether the system is indeed stable. Using the parameters from Fig. 3, stability is found everywhere within the plot for cases (a) and (b). In case (c), where the coupling $g$ is larger relative to $\lambda$, there is a region of the diagram where the phase is not stable; this is shown in Fig. 9.

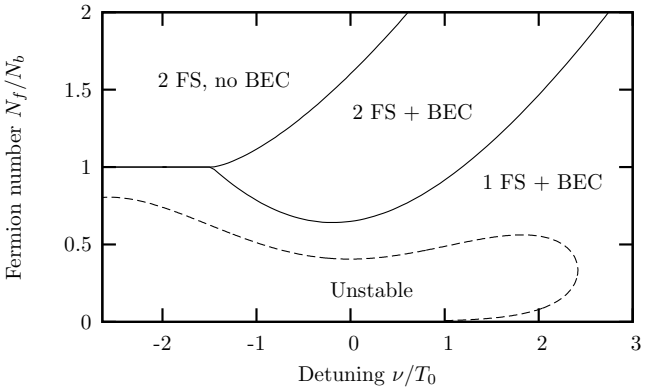


FIG. 9: The phase diagram at $T = 0$, as in Fig. 3, with couplings $\gamma^2/T_0 = 2.0 \times 10^{-2}$ and $\lambda^2 (m^b)^3 T_0 = 2 \times 10^{-3}$. The other parameters, and the labels for the three phases, are the same as in Fig. 3. The region where the phase is unstable, as determined in the Appendix, is indicated.

For large $|\nu|$ the attractive coupling from the diagram (A.7) is suppressed by a factor $1/\nu^2$ as described above, so that the system becomes stable. (The region for large negative $\nu$ is not visible on this plot.) For intermediate values of $|\nu|$, the induced coupling becomes larger than the intrinsic coupling, $\lambda$, and it is the competition between the two diagrams (A.7) and (A.8) that determines the stability.

Stability is therefore favored by a higher $N_f/N_b$, since this increases $k_0^\Psi$ and hence the phase space for the diagram (A.8). The other diagram, (A.7), increases more slowly with $k_0^\Psi$ since the internal fermion lines are restricted to be at the Fermi surface. For intermediate $|\nu|$ and very small $N_f/N_b$, on the order of $10^{-3}$, the instrinsic interaction once more dominates the induced and the system is stable. This region is too small to be seen in Fig. 9.

An analysis similar to that carried out in Ref. 25 could be performed to determine the stabilities of the alternative, mixed phases. It should be noted, however, that, as can be seen in Fig. 9, the boundaries between the three phases are not disturbed at the parameters we have considered.

Furthermore, the analysis above shows that increasing the coupling $g$ (or equivalently $\gamma^2/T_0$) beyond the value used in Fig. 9 would increase the value of $|\nu|$ required for stability at small $N_f/N_b$ (*i.e.* extend the unstable region to larger $|\nu|$), but would not decrease the stability at intermediate $|\nu|$. This follows from the fact that the latter is determined by the competition between the two diagrams (A.7) and (A.8), whose relative magnitude does not depend on $g$. We therefore expect that, for a broad Feshbach resonance, there remains a large region of sta-

bility for intermediate values of $|\nu|$, similar to that in Fig. 9.


[1] W. C. Stwalley, Phys. Rev. Lett. **37**, 1628 (1976).
[2] E. Tiesinga, B. J. Verhaar, and H. T. C. Stoof, Phys. Rev. A **47**, 4114 (1993).
[3] S. Jochim, M. Bartenstein, A. Altmeyer, G. Hendl, S. Riedl, C. Chin, J. Hecker Denschlag, and R. Grimm, Science **302**, 2101 (2003).
[4] M. Greiner, C. A. Regal, and D. S. Jin, Nature (London) **426**, 537 (2003).
[5] M. W. Zwierlein, C. A. Stan, C. H. Schunck, S. M. F. Raupach, S. Gupta, Z. Hadzibabic, and W. Ketterle, Phys. Rev. Lett. **91**, 250401 (2003).
[6] L. Radzihovsky, J. Park, and P. B. Weichman, Phys. Rev. Lett. **92**, 160402 (2004).
[7] M. W. J. Romans, R. A. Duine, S. Sachdev, and H. T. C. Stoof, Phys. Rev. Lett. **93**, 020405 (2004).
[8] A. G. Truscott, K. E. Strecker, W. I. McAlexander, G. B. Partridge, and R. G. Hulet, Science **291**, 2570 (2001).
[9] F. Schreck, L. Khaykovich, K. L. Corwin, G. Ferrari, T. Bourdel, J. Cubizolles, and C. Salomon, Phys. Rev. Lett. **87**, 080403 (2001).
[10] C. A. Stan, M. W. Zwierlein, C. H. Schunck, S. M. F. Raupach, and W. Ketterle, Phys. Rev. Lett. **93**, 143001 (2004).
[11] S. Inouye, J. Goldwin, M. L. Olsen, C. Ticknor, J. L. Bohn, and D. S. Jin, Phys. Rev. Lett. **93**, 183201 (2004).
[12] M. P. A. Fisher, P. B. Weichman, G. Grinstein, and D. S. Fisher, Phys. Rev. B **40**, 546 (1989).
[13] S. Sachdev, *Quantum Phase Transitions*, Cambridge University Press, Cambridge (1999).
[14] H. Yabu, Y. Takayama, and T. Suzuki, Physica B **329-333**, 25 (2003).
[15] R. A. Duine and H. T. C. Stoof, Phys. Rep. **396**, 115 (2004).
[16] C. A. Regal and D. S. Jin, Phys. Rev. Lett. **90**, 230404 (2003).
[17] Y. Ohashi and A. Griffin, Phys. Rev. Lett. **89**, 130402 (2002).
[18] J. M. Luttinger and J. C. Ward, Physical Review **118**, 1417 (1960).
[19] M. Potthoff, cond-mat/0406671 (2004).
[20] A. A. Abrikosov, L. P. Gorkov, and I. E. Dzyaloshinski, *Methods of Quantum Field Theory in Statistical Physics*, Dover Publications Inc., New York (1975).
[21] J. A. Hertz, Phys. Rev. B **14**, 1165 (1976).
[22] A. J. Millis, Phys. Rev. B **48**, 7183 (1993).
[23] T. Senthil, S. Sachdev, and M. Vojta, Phys. Rev. Lett. **90**, 216403 (2003); T. Senthil, M. Vojta and S. Sachdev, Phys. Rev. B **69**, 035111 (2004).
[24] V. Gurarie, L. Radzihovksy, and A. V. Andreev, cond-mat/0410620 (2005).
[25] L. Viverit, C. J. Pethick and H. Smith, Phys. Rev. A **61**, 053605 (2000).
[26] H. P. Büchler and G. Blatter, Phys. Rev. A **69**, 063603 (2004).
[27] Note that there is one implicit (three-dimensional) momentum integral in each of the first three terms, but two (three) in the term in $g$ ($\lambda$).
[28] Explicitly, $\theta_k$ is the angle parametrizing the unitary transformation from the fermions $f$ and $\psi$ in (4.1) to the fermions $F$ and $\Psi$ in (4.2).